B B

UB-HEX-94-04
SW 9425

Intermediate mass fragment emission by ^{197}Au projectile at relativistic energy in nuclear emulsion

P. L. Jain, G. Singh and A. Mukhopadhyay
High Energy Experimental Laboratory
Department of Physics
State University of New York at Buffalo
Buffalo, New York 14260

May 27, 1994

abstract

The charge distribution of multifragment decays of ^{197}Au projectile at 10.6A GeV in nuclear emulsion is fitted with a power law. The correlations between the charges emitted are given as a function of the total charge confined in fragments Z_{bound} for $Z \geq 2$, which is a measure of the violence of the collision. The observables of the present experiment are compared to the ^{197}Au beam at 600A MeV in the domain of limiting fragmentation and they are also reproduced by the predictions of the statistical and the percolation models. Small changes in the values of some of these observables are revealed in the two energies.

PACS Numbers: 24.60Ky, 25.70.Np, 25.75+r

In relativistic heavy ion collisions, the compression of nuclear matter results in the production of particles and the system expands and disassembles into multifragments. Multifragmentation has been considered to be one of the most important aspects of heavy ion collisions since it has been speculated that the decay of a highly excited nuclear system might carry information about the equation of state and the liquid–gas phase transition of low density nuclear matter. Recently, there has been a considerable progress in the study of nuclear multifragmentation in heavy ion collisions where excited nuclei decay by emitting several intermediate mass fragments (IMFs) [1, 2], but as yet we are not aware of the exact nature of these decays. Competing models suggest different decay mechanisms and experiments have yet to discriminate between several theoretical scenarios which range from the sequential decay of compound nucleus [3,4] to statistical nuclear models [5,6,7] and exotic ones

(To appear in PRC)

like large fluctuations in the region of mechanical instability [8]. To decide which processes actually occur, multifragment emission is being extensively studied in heavy ion collisions. So far, the majority of the experiments have been performed electronically and the highest projectile energy has been < 1A GeV. Recently, the ALADIN collaboration [2] at GSI studied the multifragmentation of ^{197}Au projectiles at 600A MeV on different targets and compared their results successfully with the statistical [5,6,7] and percolation models [9,10]. They concluded that there was a large degree of equilibrium in the decay system of the excited spectator at different impact parameters. At still higher energy, if the excitation energy of disassembling nucleus is lowered to the binding energy, then it may be energetically favourable for the system to decay into multifragments. In this paper, we are presenting for the first time the production of IMFs from ^{197}Au beam at the largest available energy of 10.6A GeV (an unexplored energy region – a factor of about twenty higher as compared to the GSI energy) from Brookhaven National Laboratory (BNL) in nuclear emulsion with a 4π configuration. In order to compare our high energy data with the low energy [2], we selected the same observables of the fragment distributions at the same energy deposition of these two beams. There are slight differences in the values of some of the observables. For better understanding of the multifragmentation mechanism and disentangling various available models proposed for multifragmentation, we will compare various observables in the two beams and with the predictions of statistical [5,6] and percolation [9,10] models by using for the input the size and excitation energy values of fragmenting source of low energy experiment as discussed in Refs. [2,6].

By following along the primary tracks of ^{197}Au ion at 10.6A GeV from BNL (Experiment No. 875) in a freshly prepared stack of Fuji emulsions, we observed about 1500 nuclear interactions within the first few cms. For the present analysis, we selected 1097 peripheral events having at least one projectile fragment of charge $Z \geq 2$. In each event, the charges of the PFs were determined by a combination of several methods, which included grain, gap and $\delta-$ray density and for very heavy fragments the technique of relative track width [11] was used. For a $\delta-$ray count, each track length followed was more than 0.5cm. The $\delta-$ray density measurements for fragments up to $Z = 20$ are shown in Fig. 1(a). At high energy, spectator protons from the projectile in their peripheral collisions are produced in an angle $\theta_{PF} \approx 1^0$ given by the Fermi momentum. Alpha particles are by far the most abundant fragments and are relatively easy to recognize from the grain density measurements in emulsion. From $\delta-$ray count, we determined the charges of PFs of $3 \leq Z \leq 20$ as shown in Fig. 1(a), with a charge resolution of about 0.5 charge units (cu) for $3 \leq Z \leq 7$, 0.75 cu for $8 \leq Z \leq 12$, 1.5 cu for $13 \leq Z \leq 20$, 2 cu for $20 \leq Z \leq 40$ and 3 cu for $Z > 40$. In Fig. 1(b) is shown the charge distribution of all the PFs from $Z = 1$ to 78 and this distribution follows an inverse power law with an exponent value of $\tau = -2.74 \pm 0.11$ up to $1 \leq Z \leq 24$. In drawing Fig. 1(b), we have eliminated all the fission events which are only < 1%.

At high energy, it is easy to distinguish between spectator proton tracks from the projectile nucleus and those from the target nucleus in emulsion. Information about the impact parameter and energy deposition for individual collisions may be achieved through a variety of techniques. For example, Hubele et al. [2] employed a new parameter Z_{bound} related to the size of the projectile spectator (i.e., $Z_{bound} = \sum_{Z\geq 2} Zn(Z)$, where $n(Z)$ is the multiplicity of different fragments of charge Z). This quantity is a measure of the bound charge in a cluster with $Z \geq 2$ and is complementary to the number of $Z = 1$ particles (N_p) which we used in Refs. [11] and [12]. The nearly linear relation observed between N_p

and Z_{bound} indicates that the larger value of N_p corresponds to a smaller value for Z_{bound} and to the larger violence of collision with a larger energy deposited in the excited spectator. Thus, a weak anticorrelation is expected for peripheral interactions. At still higher excitation, the projectile totally disassembles into light fragments such as α-particles and nucleons. The correlation between Z_{max} and Z_{bound} within an event in a three dimensional representation is given in Fig. 1(c) data showing the frequency of different fragments. For smaller impact parameter, the intensity where only one fragment ($Z_{max} = Z_{bound}$) is observed is strongly reduced while for large impact parameter, the intensity of single fragment ($Z_{max} = Z_{bound}$) is relatively large. Fig. 2(a) shows a scatter plot of the correlation between Z_{max} as well as $< Z_{max} >$ vs. Z_{bound} for the whole data set. Z_{max} gives some insight into how the projectile breaks apart. By definition, Z_{bound} is always larger than or equal to Z_{max} with the result that all the points are located on or below the diagonal. Any symmetric fission group should appear near $Z_{max} \approx 40$ and $Z_{bound} \approx 79$. From the correlation between the impact parameter and the number of protons N_p [12] (or Z_{bound} here) one can infer that, in general, larger and smaller Z_{bound} events are associated with peripheral and midcentral collisions, respectively. Data points plotted on the diagonal (shown by a solid line) correspond to events where only one large fragment is present. For peripheral collisions (i.e., for large Z_{bound}), most of the Z_{max} is found near the diagonal. Here at least two fragments are present, but most of the charge is contained in one of them. The farther the data point is from the diagonal, the more equally is the charge of the remaining projectile distributed between different fragments. In Fig. 2(a) is also shown the distribution of $< Z_{max} >$ vs. Z_{bound} for this experiment with statistical errors as well as for Ref. [2] along with the theoretical predictions of statistical [5, 6] and also percolation models with the details given in Ref. [2] for the model discussed in Ref. [9]. For specific Z_{bound} in the region $40 < Z_{bound} < 70$, the values of $< Z_{max} >$ are lower than for Ref. [2], showing a possible dependence on the incident energy. For lighter charged particles, $Z < 4$, included by Ref. [2] in Z_{bound}, the acceptance of the ALADIN spectrometer used in their measurements of Ref. [2] was less than unity for charged particles with $Z < 4$ [2], however. Thus some shift in the dependencies of $< Z_{max} >$ and the other quantities in Fig. 2 upon Z_{bound} to lower values of Z_{bound} may be expected for the measurement at the lower incident energy. At the values of $Z_{bound} \approx 60$, a rapid decrease of $< Z_{max} >$ is observed. Here, the total charge is more equally distributed among two or more fragments and multifragmentation emission becomes the dominant process, where it may be associated with the formation and decay of very hot nuclei. For smaller impact parameters, Z_{max}/Z_{bound} decreases and more charge is carried by the other fragments.

In Fig. 2(b) and 2(c), we plot the average two body asymmetries $< AS >$ and $< AS1 >$ vs. Z_{bound}, where $< AS > = < (Z_{max1} - Z_{max2})/(Z_{max1} + Z_{max2}) >$ and $< AS1 > = < (Z_{max2} - Z_{max3})/(Z_{max2} + Z_{max3}) >$, and Z_{max1}, Z_{max2} and Z_{max3} are the first, second and third largest fragments, respectively in each event. In Fig. 2(b), the two body asymmetry with large Z_{bound}, $< AS > \approx 1$ decreases with the decrease of Z_{bound} (more violent collisions), while the relative asymmetry in the second and third charges, as shown in Fig 2(c) is almost constant at $< AS1 > \approx 0.25$ for a large range of Z_{bound}. In this figure, we show our data along with those of Ref. [2] and also the predictions of theoretical model calculations for low energy beam [2]. For lower Z_{bound} (≤ 40), our data points are lower than for Ref. [2]. The IMF emission with charge $3 \leq Z \leq 30$ involves a breakup process. In Fig. 2(d) is shown the distribution of $< N_{IMF} >$ as a function of Z_{bound} for all the emulsion targets (i.e. $N_h > 0$), where N_h is the number of grey and black tracks produced in the interactions with the emulsion nucleus [12]. The average value of $< N_{IMF} >= 2.68 \pm 0.10$ with a peak value of $< N_{IMF} >= 3.65 \pm 0.82$ at $Z_{bound} = 42$. Along with the present data are shown the work of Hubele et al. [2] and the predictions of theoretical models. However at the lower energy, both the overall distribution for $< N_{IMF} >$ and the peak location are shifted to lower Z_{bound} values than are observed for the high energy data, thus showing a possible incident energy dependence. The N_{IMF} emission increases with the increase of Z_{bound} due to the production of higher charge fragments and charge conservation. Events with $N_{IMF} = 7$ are observed in this data sample. The correlation of $< N_{IMF} >$ and Z_{max} with Z_{bound} reflects the size of the decaying system. In order to see the monotonic relationship between $< N_{IMF} >$ and Z_{bound} as a function of the target size, we separated the events interacting with light H, CNO ($N_h < 8$) and heavy Ag, Br ($N_h \geq 8$) targets [11]. We find that the experimental points with light and heavy targets show a universal behavior and the underlying mechanisms responsible for the magnitude of N_{IMF} and Z_{bound} are strongly correlated. This correlation is determined by the excitation energy of the primary projectile, which is exhibited uniquely through the number of $N_p = Z_0 - Z_{bound}$, where N_p is the number of spectator protons from the projectile and $Z_0 = 79$. This conclusion is supported by our previous work [12] and of others [1,2] with different targets and projectiles at different energies. Thus, the collision dynamics has a negligible effect on the correlation between N_{IMF} and Z_{bound}. From Fig. 2, we find that in spite of huge differences in their incident energies, detection techniques and different targets, only small differences in their identical fragment distributions are observed. A large energy difference between the two ^{197}Au beams is exhibited through the production of the average multiplicity of Helium isotopes, i.e., $< N_\alpha >$ as a function of Z_{bound} shown in Fig. 3(a) when compared with the low energy data as reported in Ref. [6]. We have observed events with $N_\alpha = 16$. The peak value of $< N_\alpha >$ is roughly double that measured with the ALADIN spectrometer at $E/A = 600$ MeV [6]. However, since the acceptance of the ALADIN spectrometer is considerably less than unity for $\alpha-$particles, it is not clear to what extent the $\alpha-$multiplicities actually differ. We note that our $\alpha-$multiplicities are similar to those obtained in other emulsion measurements at comparable energies [13].

As Z_{bound} is related to the excitation energy of the projectile and hence to the violence of the collision in the formation of N_{IMF}, we have divided Z_{bound} into three different groups: L_1, L_2 and L_3 for $2 \leq Z_{bound} \leq 26$, $27 \leq Z_{bound} \leq 55$ and $Z_{bound} \geq 56$, respectively. In Fig. 3(b), we show the normalized frequency distribution of N_{IMF} for the three different groups; L_1 and L_3 behave almost identically with $< N_{IMF} >= 1.61 \pm 0.13$ and 2.07 ± 0.12, respectively, but medium group L_2 has $< N_{IMF} >= 2.98 \pm 0.18$ and is different from L_1 and L_3 groups. Similar behavior was also observed in ^{84}Kr and ^{238}U beams [12]. The average values of the total charge $< \Sigma Z >$ of all PFs with $Z \geq 3$ for L_1, L_2 and L_3 are 8, 28 and 60, respectively.

We have observed that the multifragmentation process follows a power law behavior and this law has also been observed in the clustering size distribution in the percolation models [9,10]. Campi [10] has suggested the method of moments correlation as a tool to discriminate beteween different fragmentation mechanisms. Following him we studied the charge distributions by the event-by-event moments. We find that Z_{bound} is strongly correlated with S_0, where $S_0 = \Sigma Z$, and the sum runs for all the fragments minus the largest charge fragment. This is shown in Fig. 4(a) and the percolation model exhibits the same kind of correlation [10]. The second moments [10] are defined by $S_2^j = \Sigma Z^2 n^j(Z)$, where $n^j(Z)$ is the multiplicity of different fragments in the jth event. The sum runs over all fragments excluding the heaviest one produced in the event and is normalized by $Z_0 = 79$. Campi has investigated the conditional moments of the fragment size distribution. Plotted in Fig. 4(b) is the charge of the largest fragment $\ln Z_{max}$ vs. the normalized second moment $< \ln S_2 >$ (excluding the largest charge) for three different groups of Z_{bound} (L_1, L_2 and L_3). According to percolation model (for critical behavior), such a plot should give rise to two branches: one from simultaneous breakup and the other from sequential decay, both of which are observed here. The events with highest multiplicity are in the lower branch ($Z_{bound} < 26$) with low Z_{max}, while events with the lowest multiplicity ($Z_{bound} > 56$) are associated with the upper branch with a high value of Z_{max}. Events with $26 \leq Z_{bound} \leq 56$ lie in between both the branches. In order to obtain a better insight into the shape of the fragment size distribution through Z_{bound}, we examined the average behavior of the relative variance $< \gamma_2 >= S_2 S_0 / S_1^2$ vs. Z_{bound}. This is shown in Fig. 4(c) for different Z_{bound}, with $< \gamma_2 >= 1.5$ near $Z_{bound} \approx 60$. Here, the singly charged particles have been excluded. If all the fragments in an event have the same size, then γ_2 will reach its lower limit of $\gamma_2 = 1$. Our data approximately coincide with ^{197}Au beam data [2] at 600A MeV for lower value of $Z_{bound} (< 50)$ and are also reproduced by the predictions of theoretical models [6,9,10] but the peak value of $< \gamma_2 >$ and its distribution beyond $Z_{bound} > 50$ is different, thus showing the effect of their projectile energy differences. The form of the curve in both the beams is the same proving once again that the same mechanisms are responsible for fragment production.

We conclude that multifragment emission is a dominant decay channel of the projectile ^{197}Au at 10.6A GeV, which peaks at $Z_{bound} = 42$. The universal dependence of $< N_{IMF} >$ on Z_{bound} suggests that Z_{bound} is related to the excitation energy of the projectile spectator. This is exhibited from simple evaporation to the total disintegration of the nuclear system irrespective of the projectile incident energy as well as the target size. Fragment size distribution exhibits similar features to those known in percolation models. The universal dependence of $< N_{IMF} >$ on Z_{bound} suggests the establishment of a thermalized source in ^{197}Au induced reactions. In spite of the huge differences in their (i) incident energies, (ii) detection techniques and (iii) different targets, nearly identical fragment distributions are observed (for $Z \geq 3$) and are also reproduced through the calculations of statistical [6] and percolation [2, 9, 10] models.

We are thankful to the BNL technical staff for their help in the exposure of emulsion stacks. Thanks to Prof. Y. Takahashi and Prof. G. Romano for their help in the preparation and development of the emulsion stack and to Dr. D. Beavis for his help in the exposure of the stack. This work was supported by D.O.E. through Grant No. DE-FGO2-90ER40566.

References

[1] Y. D. Kim *et al.*, Phys. Rev. Lett. **63**, **494** (1989); Blumenfeld *et al.*, *ibid.* **66**, 576 (1991); E. Piasecki *et al.*, *ibid.* **66** 1291 (1991); D. R. Bowman *et al.*, *ibid.* **67**, 1527 (1991).

[2] C. A. Ogilvie *et al.*, Phys. Rev. Lett. **67**, 1214 (1991); K. Hagel *et al.*, *ibid.* **68**, 2141 (1992); J. Hubele *et al.*, Z. Phys. **340**, 263 (1991; J. Hubele *et al.*, Phys. Rev. **C46**, R1577 (1992); P. Kreutz et al., preprint GSI 92-23.

[3] W. A. Friedman and W. G. Lynch, Phys. Rev. **C28**, 16 (1983); W. A. Friedman, Phys. Rev. C42, 667 (1990).

[4] R. J. Charity et al., Nucl. Phys. **A483**, 371 (1988).

[5] D. H. E. Gross, Rep. Prog. Phys. **53**, 605 (1990) and references therein; H. R. Jaqaman and D. H. E. Gross, Nucl. Phys. **A524**, 321 (1991).

[6] B. A. Li, A. R. DeAngelis and D. H. E. Gross, Phys. Lett. **B303**, 225 (1993).

[7] H. W. Barz, J. P. Bondorf, R. Donangelo and H. Schulz, Phys. Lett. **B169**, 318, (1986), J. Bondorf et al., Nucl. Phys. **A444**, 460 (1985).

[8] G. Bertsch and P. J. Siemens, Phys. Lett. **B126**, 9 (1983); C. J. Pethick and D. J. Ravenhall, Nucl. Phys. **A471**, 19c (1987)

[9] W. Bauer, Phys. Rev. **C38**, 1297 (1988); W. Bauer et al., Ann. Rev. Nucl. Sci. **42**, 77 (1992); J. D. Desbois, Nucl. Phys. **A466**, 724 (1987).

[10] D. Stauffer, Phys. Rep. **54**, 1 (1979); X. Campi, Phys. Lett. **B208**, 351 (1988) and J. Phys. **19**, 917 (1986); X. Campi and H. Krivine, Z. Phys. **A344**, 81 (1992).

[11] P. L. Jain, G. Singh and M.S. El-Nagdy, Phys. Rev. Lett. **68**, 1656 (1992) and references therein.

[12] P. L. Jain and G. Singh, Phys. Rev. **C46**, R10 (1992); *ibid.* **C47**, 2382 (1993).

[13] C. J. Waddington, to appear in Int. J. Mod. Phys. E (1993).

Figure Captions

Fig. 1 (a) Frequency distributions of $\delta-$rays of the PFs of $3 \leq Z \leq 20$ in nonfissile ^{197}Au events. Dashed cureves are free hand drawn for the most probable value. (b) Frequency distribution of the PFs of all charges for $Z = 1 - 78$ for the whole data set used . Solid curve is a power fit to the data points up to $Z = 24$ (see text). (c) Correlation between the maximum charge Z_{max} observed within an event for fixed values of Z_{bound} in a three dimensional representation.

Fig. 2 (a) Scatter plot of Z_{max} as a function of Z_{bound} for the whole data sample with diagonal as a solid line. Solid points (•) represent a plot of $< Z_{max} >$ and Z_{bound}. (∘) points for Ref. [2] and (■) correspond to the predictions of statistical [6] and (□) percolation [2,9] models. (b) $< AS >$ versus Z_{bound}. (c) $< AS1 >$ versus Z_{bound}. For the definitions of $< AS >$ and $< AS1 >$, see text. (d) The average number of fragments $< N_{IMF} >$ as a function of Z_{bound} for events with: (i) $N_h \geq 0$ (•), (ii) $N_h < 8$ (△) and (iii) $N_h \geq 8$ (▲), (iv) Data (∘) from Ref. [2] at 0.6A GeV. (v) Data compared with the calculation of statistical (■) and percolation (□) models. (∘) Ref. [2].

Fig. 3 (a) The average multiplicity of Helium isotopes $< N_\alpha >$ as a function of Z_{bound} (•). (b) Normalized frequency distributions of the fragments $< N_{IMF} >$ of charges $3 \leq Z \leq 30$ for different values of Z_{bound}. Symbols used here are for: L_1 (+), L_2 (*) and L_3 (o) groups. Dashed curves in this figure are drawn to guide the eye.

Fig. 4 (a) Correlation between S_0 and Z_{bound}. (b) A variation of $\ln Z_{max}$ as a function of $< \ln S_2 >$ for three groups of Z_{bound}. (c) $< \gamma_2 >$ versus Z_{bound}. This experiment (•), (∘) experiment of Hubele et al. [2] and compared with the calculation of statistical (■) [6] and percolation (□) models [2,9].

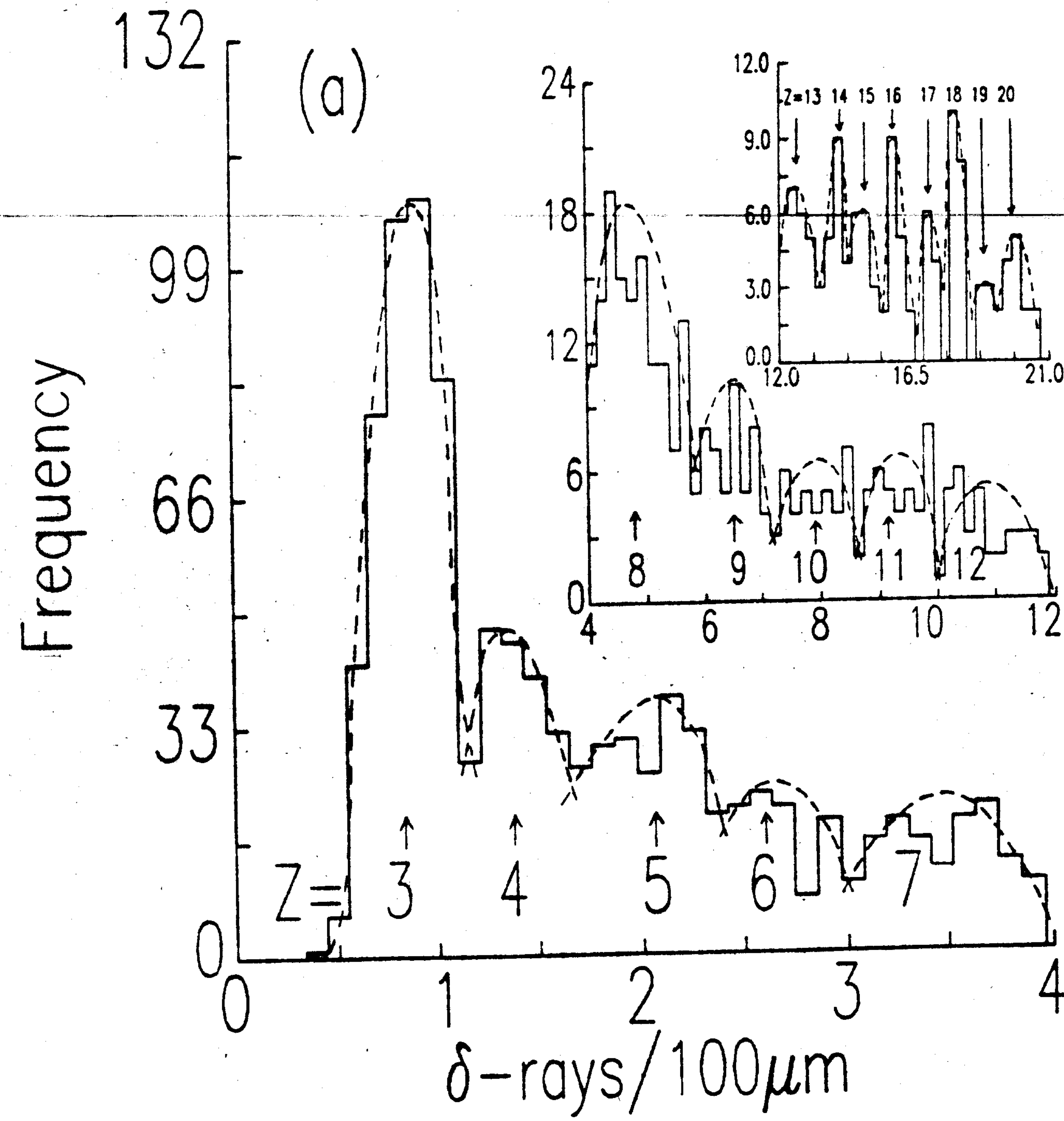

Jain et al. Fig. 1(a)

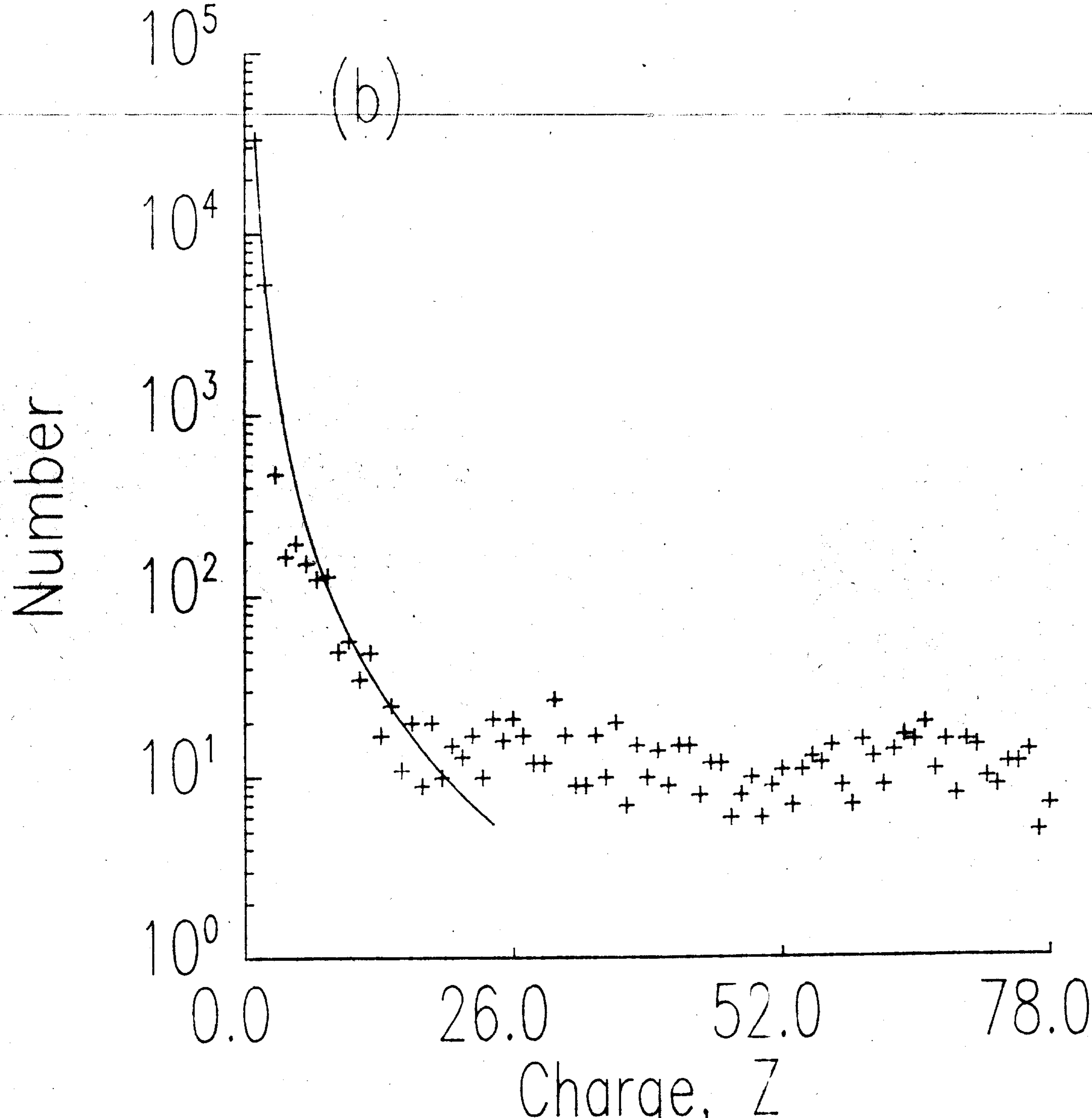

Jain et al. Fig. 1(b)

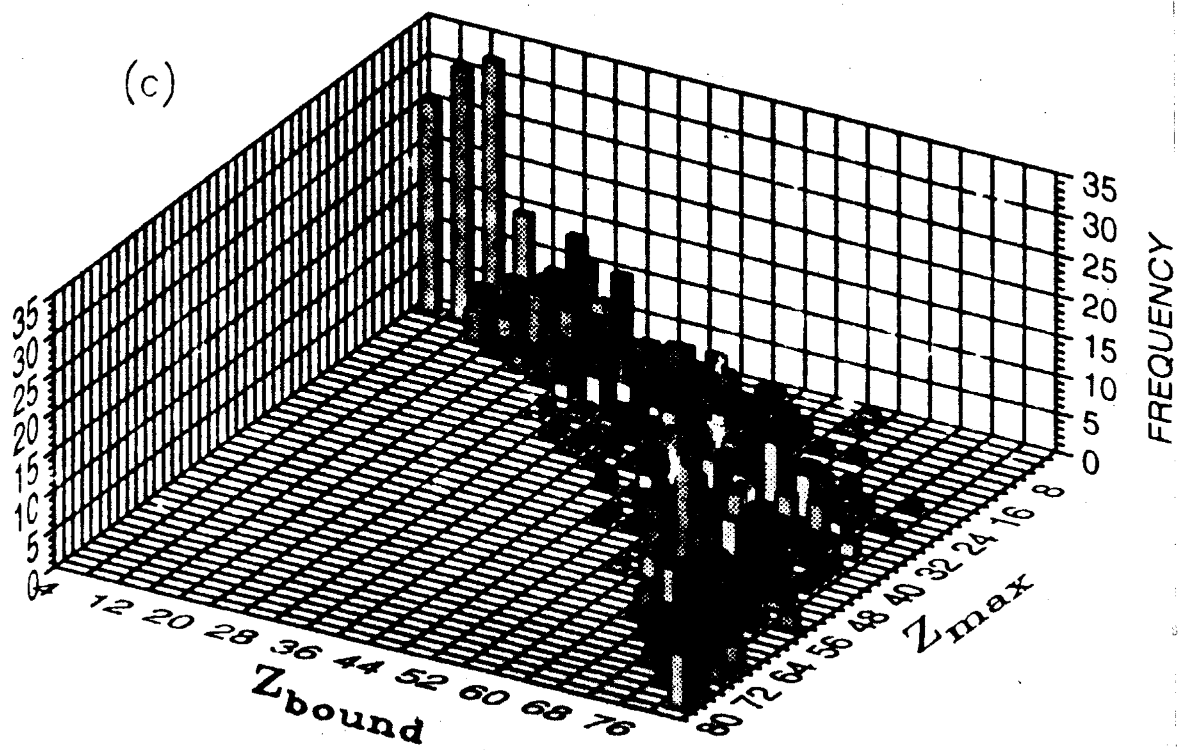

Jain et al. Fig. 1(c)

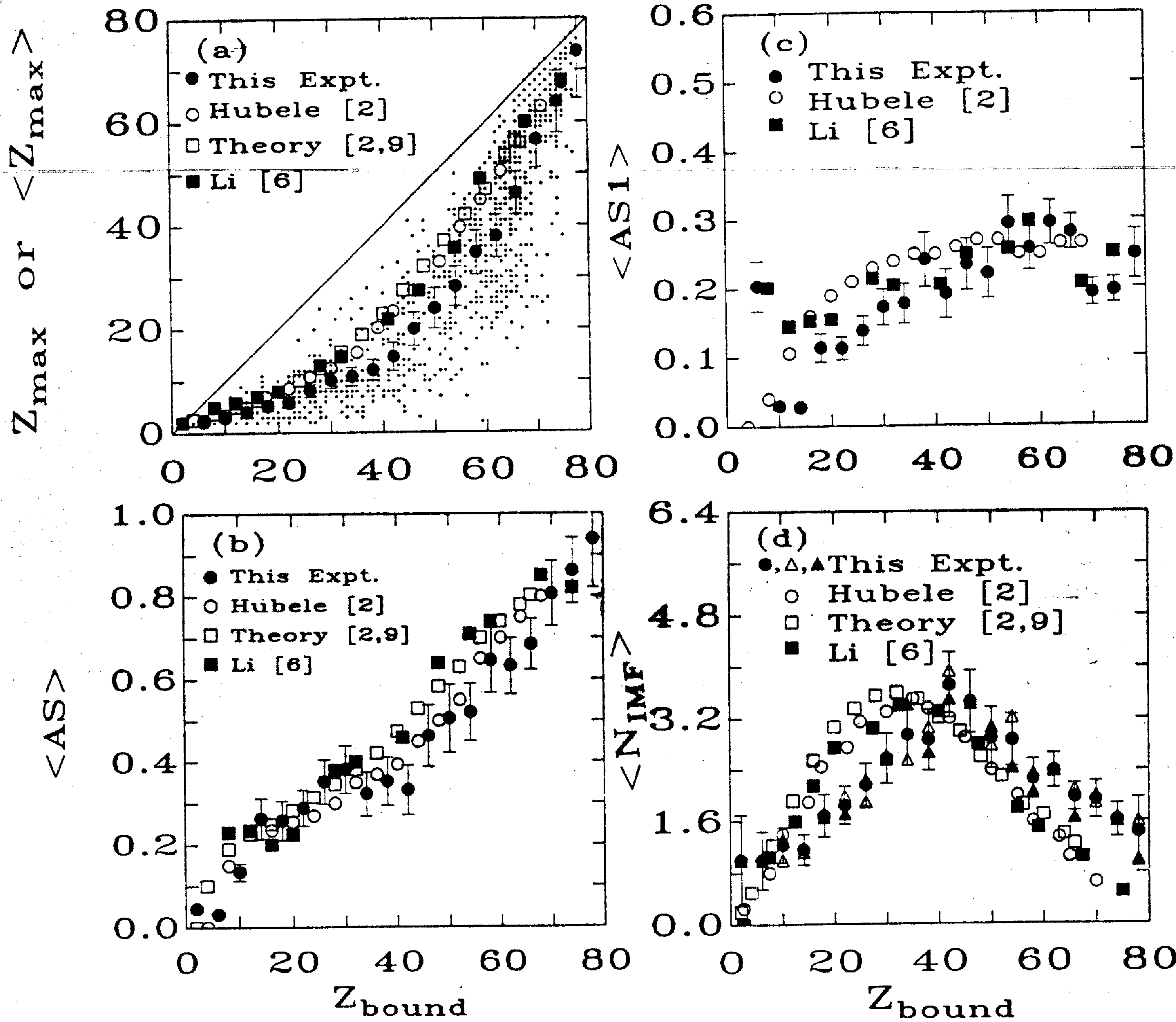

Jain et al. Fig. 2

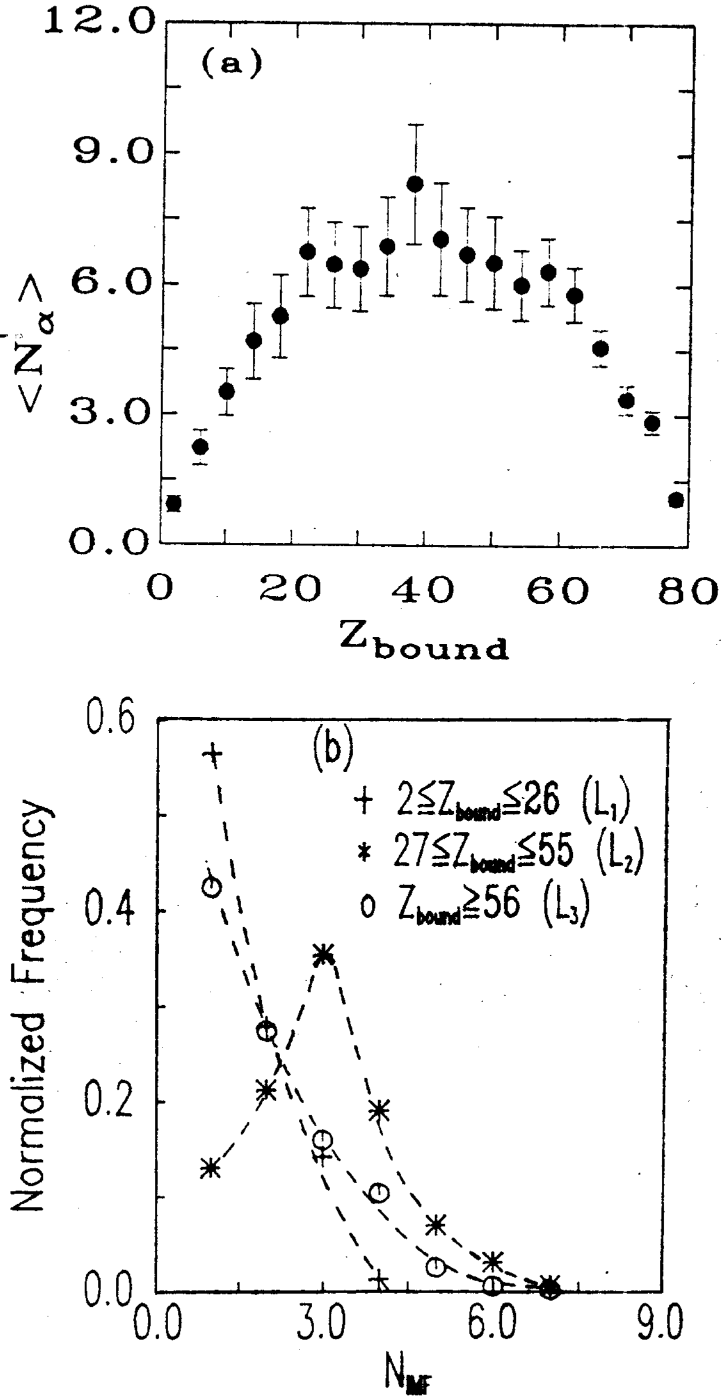

Jain et al. Fig. 3

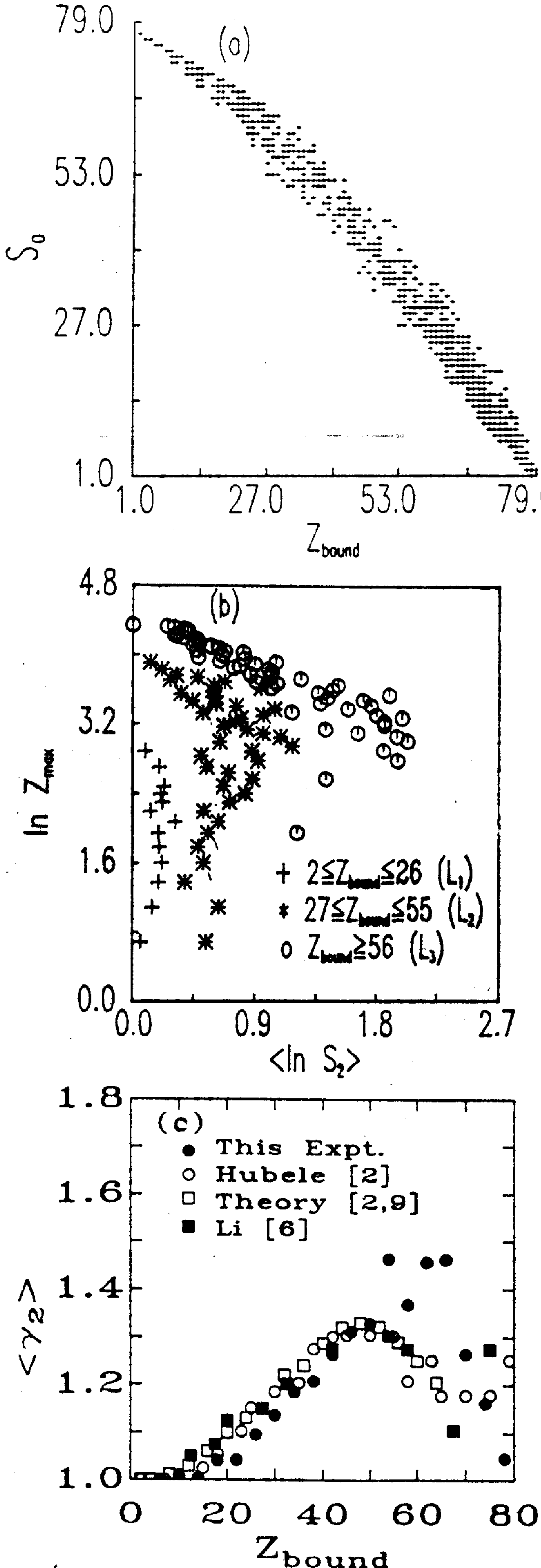

Jain et al. Fig. 4